Structures, Photoluminescence and Theoretical Studies of Two Zn^{II} Complexes with Substituted 2-(2-Hydroxyphenyl)benzimidazoles

Yi-Ping Tong,[a,b] Shao-Liang Zheng,*[a] and Xiao-Ming Chen*[a]

Keywords: Density functional calculations / N,O ligands / Photoluminescence / Pi interactions / Zinc

Two new Zn^{II} complexes of 2-(2-hydroxyphenyl)benzimidazole (Hpbm), and 5-amino-2-(1*H*-benzoimidazol-2-yl)phenol (Hapbm), namely $[Zn(pbm)_2]$ (**1**), and $[Zn(apbm)_2]\cdot C_2H_5OH\cdot H_2O$ (**2**), as well as the ligands themselves, have been prepared and characterized by X-ray crystallography and photoluminescence studies. Both **1** and **2** are neutral, mononuclear molecules that display strong photoluminescence in the blue regionand thus may serve as candidates for blue-light-emitting electroluminescent materials. The electronic transitions in the photoluminescent processes have also been investigated by means of time-dependent density functional theory (TDDFT) energy level and molecular orbitals analyses, which show that their absorption and luminescent properties are ligand-based.

Introduction

Since the first report of a double-layer green organic electroluminescence (EL) device based on Alq_3 (Hq = quinolin-8-ol) in 1987,[1] metal chelate complexes of Al^{III}, B^{III}, and Zn^{II} have been extensively investigated for their electroluminescent properties.[2,3] Unfortunately, few systematic investigations of the luminescence properties of these complexes have been carried out as extensive structural information is only now becoming available[4,5] and computational techniques have only recently allowed reliable calculations of larger molecules.[5,6] For example, $[Zn(pbt)_2]_2$ [Hpbt = 2-(2′-hydroxyphenyl)benzothiazole] has been studied as an excellent white EL material,[7] even though its molecular structure and electronic characteristics based on the density functional theory (DFT) calculations have only recently been reported.[5]

Although blue-light-luminescent coordination complexes have been an active research field for two decades,[2,8–10] stable and strong blue-emitting metal complexes are still rare, unlike the other basic components of white emission (red and green). It has been shown that some d^{10} metal complexes with N,O-donor ligands may have the high glass transition temperatures required for stable light-emitting diodes and demonstrate nice blue-emitting EL properties.[2,3,5] Among them, Zn^{II} complexes have been proved to be important candidates for EL emitters for their excellent emitting properties[7] and low cost, in comparison with other d^{10} metal (e.g. Au^{I}) complexes.[10] We recently reported a class of blue/green light luminescent d^{10} metal complexes containing the new N,O-donor ligand Hophen (Hophen = 1*H*-[1,10]phenanthrolin-2-one) and the relation between molecular structure and luminescence properties with the help of X-ray single-crystal diffraction analyses and a DFT study of the ground electronic states.[11]

In our continuing efforts to design and synthesize blue-emitting materials, we now extend our focus to benzimidazole derivatives,[12] and report herein the syntheses, crystal structures, and luminescence properties of two neutral, monomeric Zn^{II} complexes, namely $[Zn(pbm)_2]$ (**1**) and $[Zn(apbm)_2]$ (**2**) [Hpbm = 2-(2-hydroxyphenyl)benzimidazole; Hapbm = 5-amino-2-(1*H*-benzoimidazol-2-yl)phenol] (Scheme 1). The electronic transitions in the photoluminescent process have also been studied by means of time-dependent density functional theory (TDDFT) calculations.

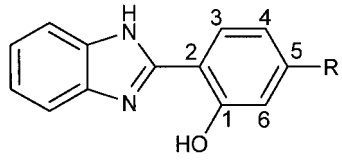

Scheme 1. The structures of Hpbm (R = H) and Hapbm (R = NH_2) with atomic labels.

Results and Discussion

Synthesis and Characterization

For practical applications, neutral coordination compounds are usually required since they may possess impor-

[a] State Key Laboratory of Optoelectronic Materials and Technologies, School of Chemistry and Chemical Engineering, Sun Yat-Sen University,
Guangzhou 510275, China
Fax: +86-20-8411-2245
E-mail: cescxm@zsu.edu.cn
[b] Department of Chemistry, Hanshan Normal College, Chaozhou 521041, China
Supporting information for this article is available on the WWW under http://www.eurjic.org or from the author.

  DOI: 10.1002/ejic.200500174

tant characteristics for the performance of their EL properties, such as a relatively high glass transition temperature and thermal stability, easy sublimation, and an ability to form thin films under vacuum.[2,3] Therefore, neutral, mononuclear metal complexes should be expected to be excellent candidates for EL materials. Similar to the other complexes that can easily form thin films under vacuum,[3] both **1** and **2** can be prepared by mixing solutions of zinc acetate and the corresponding ligand in a 1:2 ratio in ethanol. Unfortunately, single crystals for X-ray diffraction were hard to grow, thus different methods, including conventional evaporation, diffusion, and hydrothermal methods were employed. In contrast, many solid EL metal complex materials have, in fact, only been identified by their chemical compositions rather than their structures. Some of their molecular structures may be much more complicated than their empirical formulae, since they may actually be characterized to be dimeric or multinuclear structures in the solid, such as the cases of $[Znq_2]_4$,[13] $[Zn(pbt)_2]_2$,[5] and $[Zn(oz)_2]_2$ [Hoz = 2-(2′-hydroxyphenyl)-2-oxazoline].[9] This fact shows that in the absence of X-ray structures, some conclusions about their luminescence properties may be controversial.[3] Fortunately, both **1** and **2** were found to be neutral, mononuclear molecules by X-ray crystallography, thus systematic investigations of their luminescence properties can be carried out. Our trials also imply that the crystallization conditions are important.

Thermogravimetric analyses (TGA and DTG) of **1** and **2** show their high thermal stability, with decomposition temperatures of 396 and 472 °C, respectively (Figure S1 in the Supporting Information), which are similar to other EL metal-organic materials.[5,12] Preliminary trials also proved that both readily form films under vacuum.

Crystal Structures

Single-crystal X-ray diffraction analyses revealed that both **1** and **2** are neutral, mononuclear molecules with the Zn^{II} ion being tetrahedrally coordinated by two deprotonated pbm or apbm ligands (Figure 1). The dihedral angles between two ligand planes of about 89° and 88°, respectively, indicate a slight distortion from an ideal tetrahedral geometry for **1** and **2**. The N–Zn–N and O–Zn–O angles [122.7(2)° and 110.1(1)° for **1**; 116.2(1)° and 114.0(1)° for **2**] are typical for a tetrahedral geometry. The Zn–O bond lengths of 1.932(1) and 1.931(2) Å in **1** and 1.932(3) and 1.944(3) Å in **2** are slightly shorter than those documented in the literature, whereas the Zn–N bond lengths of 1.951(2) and 1.953(2) Å in **1** and 1.958(3) and 1.975(3) Å in **2** are also slightly shorter than the literature values.[5,13,14] The two crystallographically unique ligands have dihedral angles (ca. 7.2° and 7.3° for **1**; 9.9° and 20.7° for **2**) between the benzimidazole and phenolate moieties which indicate that the ligands are only slightly non-coplanar in **1**, although one ligand is significantly non-coplanar in **2**. Head-to-tail π–π stacking interactions (interligand distance of ca. 3.60 Å) exist between two molecules and give rise to a dimeric supramolecular structure in **1** (Figure 2, a). Such supramolecular dimers are stacked by edge-to-face C–H···π interactions (H···π ca. 2.75 Å) (Figure 2, b) between benzimidazole and phenolate rings of adjacent molecules, giving rise to a three-dimensional supramolecular array, while the π–π stacking interactions are in a nonparallel mode between the ligand planes of adjacent molecules, with face-to-face distances of 3.35–3.60 Å in **2** (Figure 2, c).

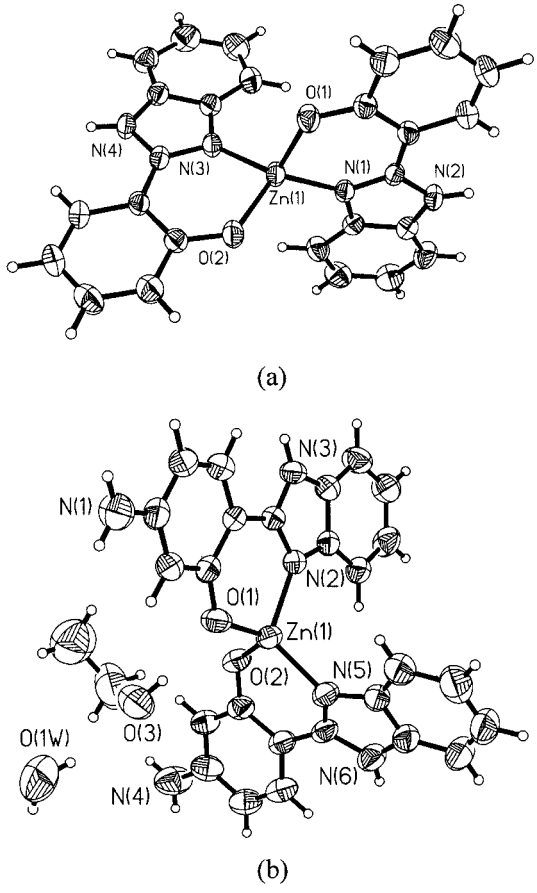

Figure 1. ORTEP views (at the 50% probability level) of **1** (a) and **2** (b).

There are also intermolecular hydrogen-bonding interactions in **1** and **2**. In **1**, the intermolecular hydrogen bonds [N(7)···O(2) = 2.796(2) Å; N(2)···O(3) = 2.822(2) Å] exist between the benzimidazole N–H groups and the deprotonated phenolate oxygen atom, furnishing a supramolecular dimer (Figure 2, a). However, the hydrogen-bonding interactions are more complicated in **2** owing to the existence of lattice water and ethanol molecules. The lattice water molecule forms two hydrogen bonds to two ethanol molecules [O(1w)···O(1) = 2.803(6) Å and O(1w)···O(2) = 2.944(6) Å], and accepts one hydrogen bond from a benzimidazole N–H group [N(1)···O(1w) = 2.855(6) Å] (Figure 3, a). Moreover, the ethanol molecule forms a hydrogen bond to the phenolate oxygen atom [O(1)···O(4) = 2.720(4) Å], and there are also intermolecular hydrogen-bonding interactions between the benzimidazole N–H groups and phenolate oxygen atoms [N(2)···O(6) = 2.791(4) Å; Figure 3, b].

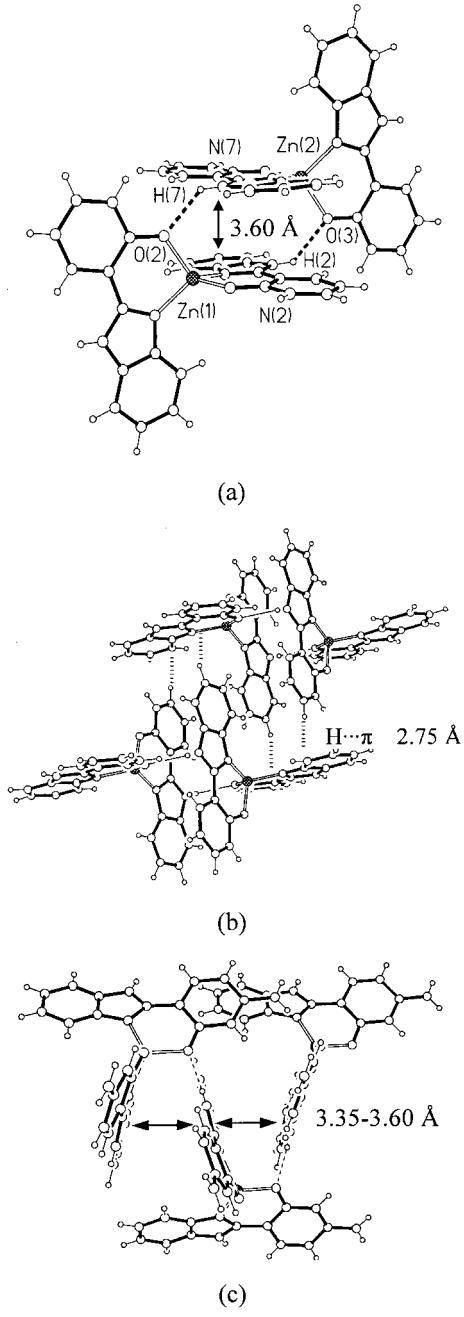

Figure 2. Perspective views of packing patterns in **1** (a, b) and **2** (c).

Neutral Hpbm and Hapbm were also crystallographically characterized. The dihedral angles (ca. 2.2° and 4.2°) between the phenolate and benzimidazole moieties for Hpbm and Hapbm indicate that both are basically coplanar. In the crystal structures of Hpbm and Hapbm, there is an intramolecular hydrogen bond between the phenolic and the imidazole groups [O(1)···N(1) = 2.554(2) Å for Hpbm and 2.563(2) Å for Hapbm] and intermolecular hydrogen bonds between the imidazole N–H groups and phenolic group oxygen atoms [N(2A)···O(1) = 2.821(3) for Hpbm and 2.826(2) Å for Hapbm] (Figure 4). These intermolecular hydrogen bonding and π–π interactions extend adja-

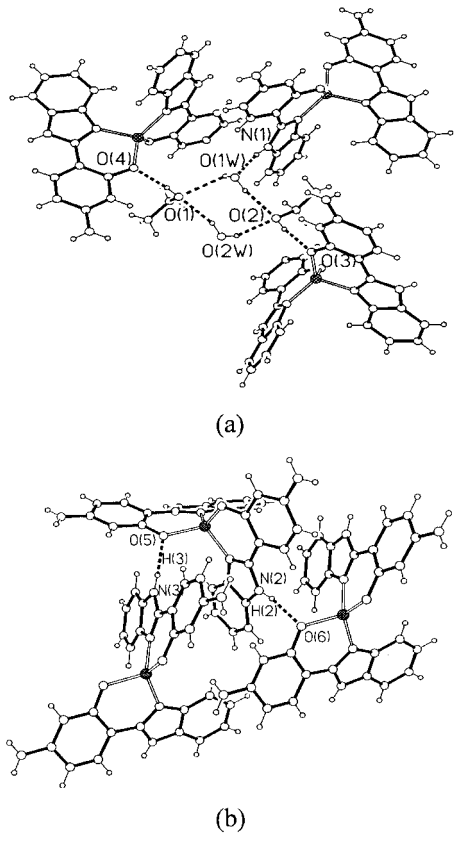

Figure 3. Perspective views of hydrogen-bonding interactions in **2**.

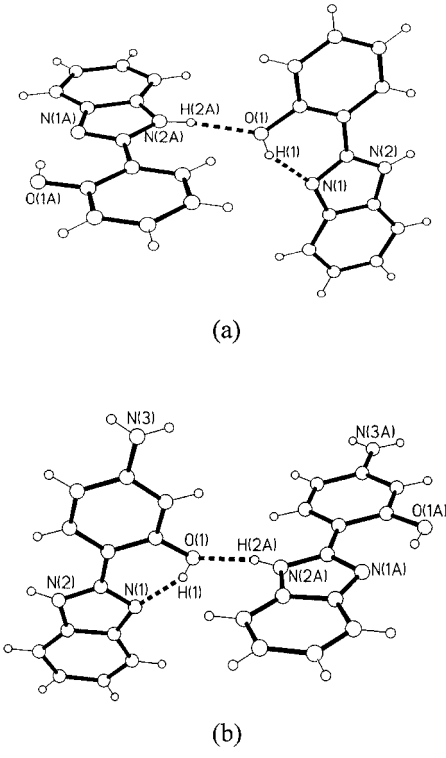

Figure 4. Perspective views of hydrogen-bonding interactions in Hpbm (a) and Hapbm (b).

cent molecules into helical chains, where each pair of adjacent molecules exhibit offset π–π stacking interactions with face-to-face distances of around 3.43 Å in Hpbm and around 3.41 Å in Hapbm (Figure 5).

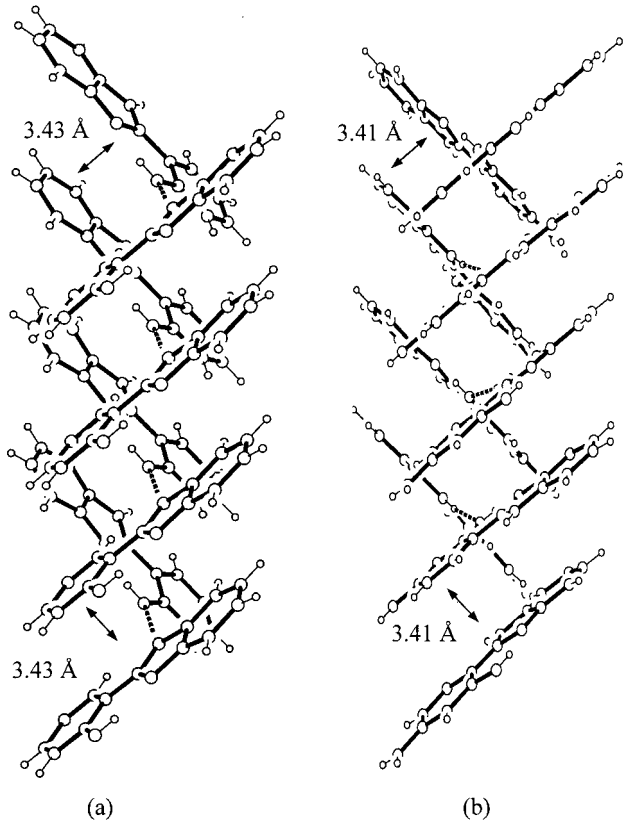

Figure 5. Perspective views of one-dimensional supramolecular arrays packed by hydrogen bonds and π–π stacking interactions in Hpbm (a) and Hapbm (b).

UV/Vis and Luminescent Spectra

The lowest-energy absorption bands of Hpbm and Hapbm in dichloromethane at 298 K occur at 323 and 325 nm, respectively, while those of their Zn^{II} complexes in dichloromethane are red-shifted slightly to 331 nm for **1** and 327 nm for **2,** with discernible shoulders at 343 and 340 nm, respectively (see Figure S2 in the Supporting Information).

The lowest-energy absorption maxima in UV spectra may correspond to S_0–S_n transitions with $n \geq 1$, as the S_0–S_1 transition may have a lower oscillator strength,[15–17] which are fully or partly transition-forbidden and too weak to be observed experimentally. According to our TDDFT calculations (Table 1), the lowest-energy absorption maxima (S_0–S_1 transition) are at 313 and 314 nm, with oscillator strengths of 0.44 and 0.78 for Hpbm and Hapbm, respectively. However, the lowest-energy absorption maximum for **1** should be attributed to the S_0–S_3 transition (wavelength: 364 nm; oscillator strength: 0.24), as the oscillator strength of the S_0–S_1 transition (wavelength: 370 nm) is only 0.04. Similarly, the lowest-energy absorption maximum for **2** can be attributed to the S_0–S_4 transition (wavelength: 344 nm; oscillator strength: 0.34), while its discernible shoulder is the S_0–S_1 transition (wavelength: 354 nm, oscillator strength: 0.16). The excited state–ground state (ES-GS) separations derived from the TDDFT calculations are in agreement with those observed experimentally.

For Hpbm and Hapbm, the S_0–S_1 transitions are mainly associated with transitions from the corresponding HOMOs to the LUMOs, as the coefficients in the configuration interaction wave functions are up to 0.63. As shown in Figure 6, the HOMOs are the π-bonding orbitals, while the LUMOs are the π*-antibonding orbitals, thus S_0–S_1 transitions can be assigned to be π→π* in nature.

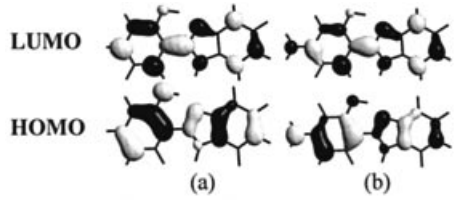

Figure 6. Contour plots of the relevant HOMOs and LUMOs of Hpbm (a) and Hapbm (b).

Similar to the corresponding ligands, the S_0–S_1 transitions of the Zn^{II} complexes are also mainly associated with transitions from the corresponding HOMOs to the LUMOs (Table S1 in the Supporting Information). As shown in Figure 7, the HOMOs are mainly the π-bonding orbitals of one deprotonated ligand, while the LUMOs are the π*-antibonding orbitals of another deprotonated ligand, thus the S_0–S_1 transitions can be assigned to be ligand-centered π→π* in nature (LCCT).

However, the S_0–S_3 transition (lowest-energy absorption maximum) of **1** is in fact mainly associated with the transitions from the corresponding HOMO–1 to LUMO and HOMO to LUMO+1, while the S_0–S_4 transition of **2** is mainly associated with the transitions from the corresponding HOMO–1 to LUMO+1 and HOMO to LUMO+1 (Table S1 in the Supporting Information), although such transitions are also assigned to be π→π* in nature.

Table 1. The calculated and experimental absorption wavelengths [nm] and their transition nature for **1**, **2**, Hpbm, and Hapbm, together with oscillator strengths.

	Transition nature	Wavelength			Oscillator strength
		Calcd.	Exp. in CH_2Cl_2	Exp. in solid	
Hpbm	π→π*	313	323	342	0.44
Hapbm	π→π*	314	325	348	0.78
1	π→π*	364	331	377	0.24
2	π→π*	344	327	368	0.34

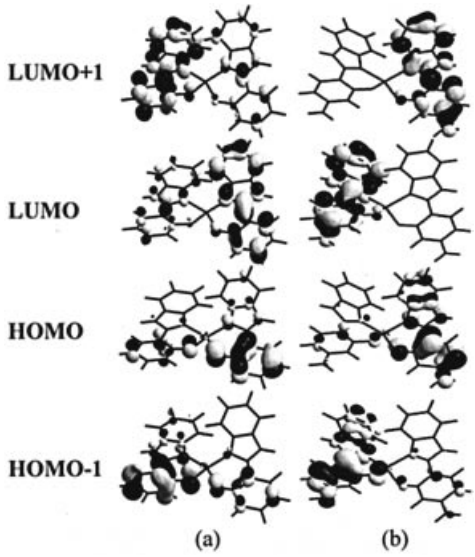

Figure 7. Contour plots of the relevant molecular orbitals (from HOMO–1 to LUMO+1) of **1** (a) and **2** (b).

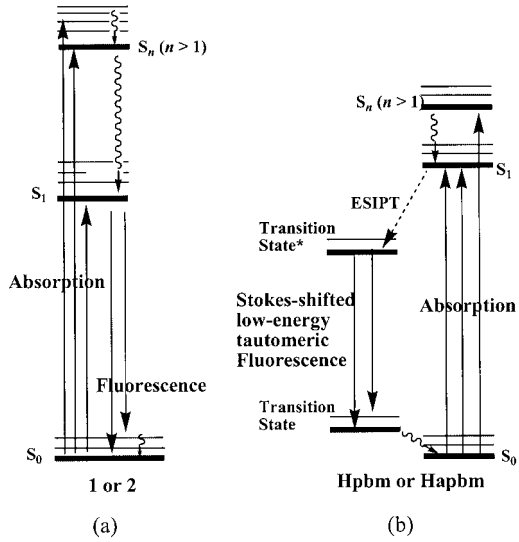

Scheme 2. The electronic transitions in the photoluminescent process of **1** or **2** (a) and Hpbm or Hapbm (b).

As has been noted,[11,18–20] the deprotonation and coordination of organic ligands to d^{10} metal ions can significantly reduce the energy gaps between the HOMOs and LUMOs. The TDDFT energy levels and experimental absorption spectra show that the S_0–S_1 energy separations of both Zn^{II} complexes become smaller than those of the corresponding ligands. According to the energy-gap law for radiationless deactivation,[17,21,22] the luminescence of the Zn^{II} complexes should be red-shifted compared with that of corresponding ligands. However, for the crystalline solid samples, Hpbm and Hapbm emit blue light with a maximum at 444 nm (λ_{ex} = 352 nm) and 426 nm (λ_{ex} = 365 nm) at 298 K, respectively, while **1** and **2** emit at 434 nm (λ_{ex} = 384 nm) and 419 nm (λ_{ex} = 379 nm), respectively (Figure 8). The violation of blue shifts can be ascribed to the excited state intramolecular proton transfer (ESIPT) of such organic compounds, which produces a strongly Stokes-shifted low-energy tautomeric fluorescence (Scheme 2).[12,23–25]

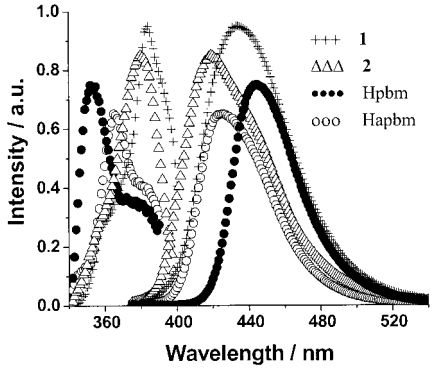

Figure 8. The excitation (left) and emission (right) spectra of **1**, **2**, Hpbm, and Hapbm in the solid state at 298 K. The corresponding excitation wavelengths, λ_{ex}, are 384, 379, 352, and 365 nm, respectively.

Moreover, the weakly electron-donating amino group can increase the electron density of the aromatic group and hence reduce the ES-GS separations slightly, consistent with the S_0–S_1 energy separations found in either the TDDFT energy levels or experimental absorption spectra of the planar Hpbm and Hapbm. On the other hand, in the absence of intramolecular hydrogen-bonding interactions (O–H···N), the 5-amino substitution may further twist the deprotonated ligand plane, as indicated by the experimental dihedral angle variation between the phenolate and benzimidazole rings of **2**, resulting in the reduction of the electron delocalization energy. Such a decrease of the delocalization energy is not favored for a π–π* transition as it may increase the energy separation. Compared with the weak electron-donating effect, the non-coplanar effect may be much stronger in **2**. In the current case, this hypothesis can be verified theoretically, as the higher ES-GS separations of **2** can be found in the TDDFT energy levels. Thus, compared to that of **1**, a significant blue shift (up to 15 nm) is observed in the luminescence of **2**. Similarly, compared to that of Hpbm, the higher emission energy of Hapbm in the non-coplanar ESIPT state is expected, although its S_0–S_1 energy separation is slightly reduced.

To the best of our knowledge, Zn^{II} complexes with aromatic heterocyclic ligands usually exhibit an emission transition that is an intraligand charge-transfer (ILCT). This is in good agreement with the assignment of the π→π* nature of the S_0–S_1 transitions for **1** and **2**. Similar to those of common Zn^{II} complexes,[18,19] the lifetimes of solid **1** and **2** are around 1.90(2) and 1.21(1) ns at room temperature.

Conclusions

Two neutral, mononuclear Zn^{II} complexes and their ligands have been prepared as possible candidates for blue-light-emitting EL materials. Systematic investigations of

electronic transitions in the photoluminescent process of all compounds have been carried out based on the X-ray structural information, as well as the TDDFT energy level and molecular orbitals analyses, and these show that their absorption and luminescent properties are ligand-based. The photophysical studies further explain the spectral variation along with the effect of complexation with Zn^{II} cations and/or amino substitution.

Experimental Section

General Remarks: All the reagents and solvents employed are commercially available and were used as received without further purification. The C, H, and N microanalyses were carried out with an Elementar Vario El elemental analyzer. ^{1}H NMR spectra were recorded with a Varian INOVA500NB spectrometer. FTIR spectra were recorded with a Bruker Vector22 spectrometer in KBr pellets in the range 4000–400 cm^{-1}. The UV/Vis spectra were recorded with a Varian Cary-100 spectrometer. The steady-state fluorescent and fluorescence lifetimes were determined with an Edinburgh Instrument FLS920 fluorescence spectrophotometer. Thermogravimetric data (TG and DTG) were collected with a Perkin–Elmer TGS-2 analyser in flowing dinitrogen atmosphere at a heating rate of 10 °C min^{-1} by heating the microcrystals.

Synthesis of Hpbm and Hapbm: They were synthesized following methods similar to those reported in the literature.[26] Salicylic acid (0.138 g, 1 mmol) and *o*-phenylenediamine (0.108 g, 1 mmol) were mixed and stirred in syrupy phosphoric acid (3 mL) at a temperature of ca. 520 K for 5 h to give white analytically pure Hpbm after recrystallization of the crude product (ca. 10% yield). X-ray quality crystals were grown by slow evaporation of a solution in $CHCl_3$ for about one week. $C_{13}H_{10}N_2O$ (210.2): calcd. C 74.27, H 4.79, N 13.33; found C 74.02, H 4.81, N 13.49. ^{1}H NMR (500 MHz, [D_6]-DMSO): δ = 13.13 (s, 1 H), 13.12 (s, 1 H), 8.04 (dd, J = 1.50, 8.00 Hz, 1 H), 7.71 (d, J = 8.00 Hz, 1 H), 7.60 (d, J = 7.50 Hz, 1 H), 7.38 (m, 1 H), 7.28 (m, 2 H), 7.03 (m, 2 H) ppm. FTIR (KBr): $\tilde{\nu}$ = 3326 (vs), 1585 (s), 1492 (s), 1417 (s), 1320 (m), 1282 (m), 1262 (s), 1133 (m), 1037 (w), 911 (w), 840 (w), 798 (w), 727 (s), 591 (w), 522 (w), 464 (w) cm^{-1}.

Hapbm was similarly synthesized by reaction of *o*-phenylenediamine (0.108 g, 1 mmol) with 4-aminosalicylic acid (0.153 g, 1 mmol). X-ray quality crystals were grown by very slow evaporation of a solution of DMF over about one month. The yield was ca. 10%. $C_{13}H_{11}N_3O$ (225.2): calcd. C 69.32, H 4.92, N 18.66; found C 69.07, H 4.81, N 18.72. ^{1}H NMR (500 MHz, [D_6]DMSO): δ = 12.96 (s, 1 H), 12.68 (s, 1 H), 7.65 (d, J = 8.10 Hz, 1 H), 7.51 (s, 2 H), 7.17 (dd, J = 3.00, 7.16 Hz, 2 H Hz,), 6.21 (dd, J = 2.10, 8.40 Hz, 1 H), 6.14 (d, J = 1.50 Hz, 1 H), 5.68 (s, 2 H) ppm. FTIR (KBr): $\tilde{\nu}$ = 3471 (m), 3381 (s), 3221 (s), 1631 (s), 1589 (s), 1553 (m), 1424 (s), 1363 (m), 1268 (s), 1198 (m), 1153 (m), 961 (w), 806 (m), 737 (s), 681 (w), 538 (w), 522 (w) cm^{-1}.

Synthesis of [Zn(pbm)$_2$] (1): A mixture of zinc acetate dihydrate (0.110 g, 0.5 mmol), Hpbm (0.210 g, 1.0 mmol), and water (10 mL) was heated in a 23-mL, Teflon-lined stainless-steel container at 110 °C for 4 d. After cooling to room temperature at a rate of 5 K per hour, the colorless crystals of **1** were isolated (yield ca. 0.17 g, 70%). $C_{26}H_{18}N_4O_2Zn$ (483.8): calcd. C 64.54, H 3.75, N 11.58; found C 64.32, H 3.84, N 11.72. ^{1}H NMR (500 MHz, [D_6]DMSO): δ = 13.34 (s, 2 H), 7.98 (d, J = 7.00 Hz, 2 H), 7.58 (d, J = 8.00 Hz, 2 H), 7.25 (d, J = 8.00 Hz, 4 H), 7.05 (q, J = 7.00 Hz, 4 H), 6.80 (d, J = 7.50 Hz, 2 H), 6.68 (t, J = 7.00 Hz, 2 H) ppm. FTIR (KBr): $\tilde{\nu}$ = 3428 (m), 1798 (w), 1567 (s), 1478 (m), 1444 (m), 1407 (m), 1311 (w), 1251 (w), 1140 (w), 876 (w), 738 (w), 654 (w) cm^{-1}.

Table 2. Crystal data and structure refinement for **1**, **2**, Hpbm, and Hapbm.

Complex	**1**	**2**	Hpbm	Hapbm
Empirical formula	$C_{26}H_{18}N_4O_2Zn$	$C_{28}H_{28}N_6O_4Zn$	$C_{13}H_{10}N_2O$	$C_{13}H_{11}N_3O$
Formula mass	483.81	577.93	210.23	225.25
Temperature [K]	293(2)	293(2)	293(2)	293(2)
Crystal system	monoclinic	orthorhombic	orthorhombic	orthorhombic
Space group	$P2_1/n$	*Pbcn*	$Pna2_1$	*Pbca*
a [Å]	10.188(1)	28.900(2)	18.236(16)	12.932(1)
b [Å]	10.010(1)	9.1250(5)	4.8061(17)	8.5641(7)
c [Å]	21.323(1)	20.062(1)	11.990(11)	19.7343(16)
β [°]	94.029(1)	90	90	90
V [Å^3]	2169.2(3)	5290.4(5)	1050.8(14)	2185.5(3)
Z	4	8	4	8
$\rho_{calcd.}$ [mg m^3]	1.481	1.451	1.329	1.369
Abs. coefficient [mm^{-1}]	1.164	0.975	0.087	0.091
F(000)	992	2400	440	944
Crystal size [mm]	0.26 × 0.13 × 0.11	0.46 × 0.24 × 0.08	0.52 × 0.36 × 0.33	0.37 × 0.23 × 0.11
Absorption correction	multi-scan	multi-scan	multi-scan	multi-scan
Index ranges	$-13 \le h \le 10$	$-37 \le h \le 36$	$-23 \le h \le 10$	$-16 \le h \le 15$
	$-12 \le k \le 12$	$-11 \le k \le 11$	$-4 \le k \le 6$	$-9 \le k \le 11$
	$-27 \le l \le 27$	$-26 \le l \le 19$	$-15 \le l \le 14$	$-25 \le l \le 20$
Reflections collected	13051	29997	4138	12220
Unique reflections	4884	6054	2138	2494
Parameters	298	359	146	154
R_{int}	0.0241	0.0599	0.0163	0.0296
Goodness-of-fit	1.050	1.047	1.041	1.072
R_1 [$I > 2\sigma(I)$]	0.0361	0.0612	0.0425	0.0566
wR_2 [$I > 2\sigma(I)$]	0.0914	0.1524	0.1023	0.1247
R_1 (all data)	0.0454	0.1015	0.0484	0.0761
wR_2 (all data)	0.0967	0.1784	0.1057	0.1336
Largest diff. peak and hole [e Å^{-3}]	0.403/–0.321	0.783/–0.425	0.152/–0.190	0.182/–0.157

Synthesis of $[Zn(apbm)_2]\cdot C_2H_5OH\cdot H_2O$ (2): A filtered solution of Hapbm (0.45 g, 2 mmol) and potassium hydroxide (0.112 g, 2 mmol) in ethanol (80 mL) was added to a solution of zinc acetate dihydrate (0.22 g, 1 mmol) in ethanol (40 mL) at a temperature of 60 °C. The mixture was kept for 4 h at this temperature, and allowed to stand overnight at room temperature. The white precipitate was filtered, washed with ethanol, and dried under reduced atmosphere over silica gel at room temperature for 3 h to give **2** as pale-yellow microcrystals. X-ray quality crystals were obtained by very slow evaporation of a solution in ethanol over about 60 days (ca. 0.29 g, 50% yield based on Zn). $C_{28}H_{28}N_6O_4Zn$ (579.0): calcd. C 58.19, H 4.88, N 14.54; found C 58.33, H 4.58, N 14.42. ^{1}H NMR (500 MHz, [D$_6$]DMSO): δ = 7.62 (d, J = 8.70 Hz, 2 H), 7.42 (d, J = 7.50 Hz, 2 H), 7.11 (t, J = 7.50 Hz, 2 H), 6.96 (t, J = 7.80 Hz, 2 H), 6.86 (d, J = 7.80 Hz, 2 H), 6.01 (dd, J = 2.10, 8.70 Hz, 2 H), 5.91 (d, J = 2.10 Hz, 2 H), 5.39 (s, 4 H). FTIR (KBr): $\tilde{\nu}$ = 3375 (s), 3334 (s), 3211 (m), 1624 (s), 1534 (s), 1478 (s), 1463 (s), 1447 (s), 1396 (w), 1348 (w), 1327 (w), 1296 (w), 1253 (m), 1213 (m), 1157 (m), 980 (w), 848 (w), 811 (w), 751 (m), 602 (w), 539 (w), 508 (w) cm^{-1}.

X-ray Crystallographic Study: Diffraction intensities for **1** and **2**, as well as Hpbm and Hapbm, were collected at 293 K on a Bruker Smart Apex CCD diffractometer (Mo-K_α radiation; λ = 0.71073 Å). Absorption corrections were applied with SADABS.[27] The structures were solved by direct methods and refined with full-matrix least-squares using the SHELXTL program package.[28] The organic hydrogen atoms were generated in ideal positions. Anisotropic thermal parameters were applied to all non-hydrogen atoms. Experimental details of the X-ray analyses are provided in Table 2, with selected bond lengths and angles listed in Table 3.
CCDC-258466 to -258468 (for **1**, **2**, and Hapbm, respectively) and -240084 (Hpbm) contain the supplementary crystallographic data for this paper. These data can be obtained free of charge from The Cambridge Crystallographic Data Centre via www.ccdc.cam.ac.uk/data_request/cif.

Calculation Details: Based on the optimized geometries (selected optimized bond lengths and bond angles are listed in Table S2 in the Supporting Information), time-dependent density functional (TDDFT) calculations were performed at the B3LYP level with a 6-31G** basis set for C, H, N, and O atoms, and effective core potentials basis set LanL2DZ for Zn atoms, employing the Gaussian03 suite of programs.[29] The electron density diagrams of molecular orbitals were obtained with the Gaussview graphics program.

Table 3. Selected bond lengths [Å] and angles [°] for **1**, **2**, Hpbm, and Hapbm.

1			
Zn(1)–O(2)	1.931(2)	Zn(1)–N(1)	1.951(2)
Zn(1)–O(1)	1.932(1)	Zn(1)–N(3)	1.953(2)
O(2)–Zn(1)–O(1)	110.1(1)	O(2)–Zn(1)–N(3)	95.3(1)
O(2)–Zn(1)–N(1)	121.0(1)	O(1)–Zn(1)–N(3)	112.6(1)
O(1)–Zn(1)–N(1)	95.7(1)	N(1)–Zn(1)–N(3)	122.7(1)
2			
Zn(1)–O(1)	1.932(3)	Zn(1)–N(2)	1.958(3)
Zn(1)–O(2)	1.944(3)	Zn(1)–N(5)	1.975(3)
O(1)–Zn(1)–O(2)	114.0(1)	O(1)–Zn(1)–N(5)	126.7(1)
O(1)–Zn(1)–N(2)	94.7(1)	O(2)–Zn(1)–N(5)	95.1(1)
O(2)–Zn(1)–N(2)	110.7(1)	N(2)–Zn(1)–N(5)	116.2(1)
Hpbm			
N(1)–C(7)	1.322(3)	N(2)–C(8)	1.372(3)
N(1)–C(13)	1.389(3)	O(1)–C(1)	1.355(3)
N(2)–C(7)	1.359(3)	C(6)–C(7)	1.457(3)
O(1)–C(1)–C(6)	121.4(2)	N(1)–C(7)–C(6)	123.4(2)
N(2)–C(7)–C(6)	124.9(2)		
Hapbm			
O(1)–C(1)	1.356(2)	N(2)–C(7)	1.354(2)
N(1)–C(7)	1.327(2)	N(2)–C(13)	1.382(2)
N(1)–C(8)	1.389(2)		
O(1)–C(1)–C(6)	121.4(2)	N(2)–C(7)–C(6)	124.7(2)
N(1)–C(7)–C(6)	123.4(2)	N(3)–C(3)–C(4)	121.0(2)

Acknowledgments

This work was supported by the National Natural Science Foundation of China (grant no. 20131020) and the Scientific and Technological Project of Guangdong Province (nos. 2003C103004, 036601, and 04205405).

[1] C. W. Tang, S. A. VanSlyke, *Appl. Phys. Lett.* **1987**, *51*, 913–915.
[2] S.-N. Wang, *Coord. Chem. Rev.* **2001**, *215*, 79–98, and references cited therein.
[3] *Handbook of Luminescence, Display Materials, and Devices* (Eds.: H. S. Nalwa, L. S. Rohwer, A. J. Heeger), American Scientific Publishers, Stevenson Ranch, Calif., **2003**, and references cited therein.
[4] a) M. Brinkmann, G. Gadret, M. Muccini, C. Taliani, N. Masciocchi, A. Sironi, *J. Am. Chem. Soc.* **2000**, *122*, 5147–5157; b) M. Cölle, R. E. Dinnebier, W. Brütting, *Chem. Commun.* **2002**, 2908–2909, and references cited therein.
[5] G. Yu, S. Yin, Y. Liu, Z. Shuai, D. Zhu, *J. Am. Chem. Soc.* **2003**, *125*, 14816–14824.
[6] a) M. D. Halls, H. B. Schlegel, *Chem. Mater.* **2001**, *13*, 2632–2640; b) P. J. Hay, *J. Phys. Chem. A* **2002**, *106*, 1634–1641.
[7] Y. Hamada, T. Sano, H. Fujii, Y. Nishio, H. Takahashi, K. Shibata, *Jpn. J. Appl. Phys.* **1996**, *35*, L1339–L1341.
[8] N. Nakamura, S. Wakabayashi, K. Miyairi, T. Fujii, *Chem. Lett.* **1994**, 1741–1742.
[9] J. Zhang, S. Gao, C.-M. Che, *Eur. J. Inorg. Chem.* **2004**, 956–959.
[10] M. Osawa, M. Hoshino, M. Akita, T. Wada, *Inorg. Chem.* **2005**, *44*, 157–1159.
[11] S.-L. Zheng, J.-P. Zhang, X.-M. Chen, Z.-L. Huang, Z.-Y. Lin, W.-T. Wong, *Chem. Eur. J.* **2003**, *9*, 3888–3896.
[12] Y.-P. Tong, S.-L. Zheng, X.-M. Chen, *Inorg. Chem.* **2005**, DOI: 10.1021/ic0501059.
[13] L. S. Sapochak, F. E. Benincasa, R. S. Schofield, J. L. Baker, K. K. C. Riccio, D. Fogarty, H. Kohlmann, K. F. Ferris, P. E. Burrows, *J. Am. Chem. Soc.* **2002**, *124*, 6119–6125.
[14] Q. Wu, J. A. Lavigne, Y. Tao, M. D'Iorio, S. Wang, *Inorg. Chem.* **2000**, *39*, 5248–5254.
[15] N. J. Turro, K.-C. Liu, M.-F. Show, P. Lee, *Photochem. Photobiol.* **1978**, *27*, 523–529.
[16] a) S.-L. Zheng, P. Coppens, *CrystEngCommun.* **2005**, *7*, 289–293; b) S.-L. Zheng, P. Coppens, *Chem. Eur. J.* **2005**, *11*, 3583–3590.
[17] J. M. Klessinger, J. Michl, *Excited States and Photochemistry of Organic Molecules*, VCH, New York, **1995**.
[18] S.-L. Zheng, J.-H. Yang, X.-L. Yu, X.-M. Chen, W.-T. Wong, *Inorg. Chem.* **2004**, *43*, 830–838.
[19] S.-L. Zheng, X.-M. Chen, *Aust. J. Chem.* **2004**, *57*, 703–712.
[20] V. W.-W. Yam, Y.-L. Pui, K.-K. Cheung, *Inorg. Chem.* **2000**, *39*, 5741–5746.
[21] N. J. Turro, *Modern Molecular Photochemistry*, University Science Books, Sausalito, CA, **1978**.

[22] D. V. Scaltrito, D. W. Thompson, J. A. O'Callaghan, G. J. Meyer, *Coord. Chem. Rev.* **2000**, *208*, 243–266.
[23] J. Waluk, *Conformational Analysis of Molecules in Excited States*, Wiley-VCH, **2000**, 83–85, and references cited therein.
[24] D. LeGourriérec, V. A. Kharlanov, R. G. Brown, W. Rettig, *J. Photochem. Photobiol. A: Chem.* **2000**, *130*, 101–111.
[25] W. E. Brewer, M. L. Martinez, P.-T. Chou, *J. Phys. Chem.* **1990**, *94*, 1915–1918.
[26] A. W. Addison, P. J. Burke, *J. Heterocycl. Chem.* **1981**, *18*, 803–805.
[27] R. Blessing, *Acta Crystallogr., Sect. A* **1995**, *51*, 33–38.
[28] G. M. Sheldrick, *SHELXTL 6.10*, Bruker Analytical Instrumentation, Madison, Wisconsin, USA, **2000**.
[29] M. J. Frisch, G. W. Trucks, H. B. Schlegel, G. E. Scuseria, M. A. Robb, J. R. Cheeseman, V. G. Zakrzewski, J. A. Montgomery, R. E. Stratmann, J. C. Burant, S. Dapprich, J. M. Millam, A. D. Daniels, K. N. Kudin, M. C. Strain, O. Farkas, J. Tomasi, V. Barone, M. Cossi, R. Cammi, B. Mennuci, C. Pomelli, C. Adamo, S. Clifford, J. Ochterski, G. A. Petersson, P. Y. Ayala, Q. Cui, K. Morokuma, D. K. Malick, A. D. Rabuck, K. Raghavachari, J. B. Foresman, J. Cioslowski, J. V. Oritz, B. B. Stefanov, G. Liu, A. Liashenko, P. Piskorz, I. Komaromi, R. Gomperts, R. L. Martin, D. J. Fox, T. Keith, M. A. Al-Laham, C. Y. Peng, A. Nanayakkara, C. Gonzalez, M. Challacombe, P. M. W. Gill, B. G. Johnson, W. Chen, M. W. Wong, J. L. Andres, M. Head-Gordon, E. S. Replogle, J. A. Pople, *GAUSSIAN03, Revision C.02*; Gaussian, Inc., Pittsburgh, PA, **2003**.

Received: February 27, 2005
Published Online: August 11, 2005

